International Journal of Heat and Mass Transfer 63 (2013) 224–232

Contents lists available at SciVerse ScienceDirect

International Journal of Heat and Mass Transfer

journal homepage: www.elsevier.com/locate/ijhmt

# Augmented boiling heat transfer on the wetting-modified three dimensionally-interconnected alumina nano porous surfaces in aqueous polymeric surfactants

Bong June Zhang [a,b,1], Jiyeon Park [b,1], Kwang Jin Kim [a,*]

[a] Department of Mechanical Engineering, Box 454027, University of Nevada, Las Vegas, NV 89154, USA
[b] Low Carbon Green Technology Laboratory, Department of Mechanical Engineering (MS312), University of Nevada, Reno, NV 89557, USA

ARTICLE INFO

*Article history:*
Received 15 October 2012
Received in revised form 23 March 2013
Accepted 23 March 2013
Available online 30 April 2013

*Keywords:*
Nano-porous surfaces
Nucleate pool boiling heat transfer enhancement
Surfactant
Surface wettability
Drop impact test
Aluminum oxide
Anodizing

ABSTRACT

Pool boiling in an aqueous surfactant solution is one of efficient approaches to increase pool boiling performance in nucleate boiling regime since additive polymer surfactants modify interfacial wetting properties between heating surface and fluids. Enhanced wetting increases bubble departure frequency and prevents bubble coalescence. Most pool boiling tests in aqueous surfactant solutions have been carried out on non-porous surfaces (plain surfaces) and heat transfer performances reported were not drastic. In this study, the Alumina Sponge-like Nano Porous Surface (ASNPS) was used as a heating surface in aqueous SDS solutions. The ASNPS's surface wetting was modified with a hydrophobic Self-Assembly Monolayer (SAM) coating. The wetting-modified ASNPS shows substantial increase in active nucleation sites through three-dimensionally interconnected porous network. Eventually, significant heat transfer enhancement (7.3 times) is achieved due to the combined effects.

For bubble motion characterization associated with surfactants, various approaches have been made using Dynamic Light Scattering (DLS), Transmission Electron Microscopy (TEM), Static Water Contact Angle (SWCA) measurements, and high speed image analysis of liquid impingement.



## 1. Introduction

Since enhanced pool boiling phenomena are closely related to bubble dynamics in heating fluid, such as bubble departure diameter and frequency, there have been various efforts to modify heating fluid properties such as surface tension, viscosity, and conductivity. Frost and Kippenhan reported nucleate pool boiling heat transfer increase in an aqueous surfactant solution [1]. Since surfactants added to heating fluid are in small amounts, the bulk properties of heating fluid are rarely influenced except surface tension, which directly influences surface wetting. Typically, enhanced wetting prevents the bubble coalescence and increases the bubble departure frequency [2]. As the bubble departure frequency increases, the latent heat from the heating surface is removed by two-phase boiling phenomena. Also, thermal boundary layers near the heating surface are perturbed and wall superheat increase is significantly suppressed. Eventually, heat transfer enhancement is achieved due to surface wetting-assisted bubble dynamics over the entire heat flux regimes [3].

Table 1 shows a summary of pool boiling results under various conditions. For most cases, pool boiling was carried out using non-porous surfaces. Heat transfer enhancement was approximately less than 150%. In general, Static Water Contact Angle (SWCA) for a plain surface is less than 90°, which is somewhat hydrophilic. When a plain surface is exposed to an aqueous surfactant solution, it becomes easily wet and shows enhanced wetting. Heat transfer enhancement using surfactant-induced hydrophilization on the non-surface treated heater is well-established in the literature [7,12–14].

In this study, we present nucleate pool boiling enhancement in polymeric surfactants with the characteristic Alumina Sponge-like Nano Porous Surface (ASNPS). The ASNPS [15,16] is fabricated by electrochemical anodic oxidation method [15,16]. It has numerous reentrant cavities, which play a role of effective vapor traps with an enhanced heating surface area. The increase in surface area can contribute to boiling incipience reduction and Heat Transfer Coefficient (HTC) increase [16]. Further, the heating surface wetting of the ASNPS is modified using a hydrophobic Self-Assembly Monolayer (SAM), which prevents liquid from flooding active nucleation sites [15]. This study has significant meaning since surface chemistry of surfactant-induced hydrophilization on the hydrophobic surface and relevant heat transfer experiments have not been introduced yet. Also, micelle formation at higher concentration of

* Corresponding author. Tel./Fax: +1 702 774 1419.
*E-mail address:* kwang.kim@unlv.edu (K.J. Kim).
[1] Fax: +1 775 784 1701.

0017-9310/$ - see front matter © 2013 Elsevier Ltd. All rights reserved.
http://dx.doi.org/10.1016/j.ijheatmasstransfer.2013.03.064

**Nomenclature**

| | |
|---|---|
| $d$ | diameter [m] |
| $h$ | heat transfer coefficient [kW/m$^2$ K] |
| $q''$ | heat flux [W/m$^2$] |
| $r$ | radius [m] |
| $T$ | temperature [K] |
| $\Delta T$ | temperature difference [K] |

**Greek letters**

| | |
|---|---|
| $\Delta$ | difference |
| $\theta$ | contact angle [°] |
| $\sigma$ | surface tension [N/m] |

**Subscripts**

| | |
|---|---|
| $l$ | liquid |
| $lv$ | liquid–vapor |
| $o$ | initial |
| $p$ | pore |
| $s$ | solid |
| $sat$ | saturation |
| $sv$ | solid–vapor |
| $sl$ | solid–liquid |
| $v$ | vapor |
| $w$ | wall |

surfactants is characterized using various spectroscopic methods such as Dynamic Light Scattering (DLS) and Transmission Emission Microscopy (TEM).

## 2. Experiment

### 2.1. Preparation of Alumina Sponge-like Nano Porous Surface (ASNPS)

Three dimensionally interconnected Alumina Sponge-like Nano-Porous Surface (ASNPS), was created using two step anodizing in 0.3 M phosphoric acid at 140 V [15,16]. The ASNPS has a hybrid porous structure consisting of smaller pores ($d_p \sim 100$ nm) and larger pores ($d_p \sim 500$ nm). Cross-sectional views reveal that the hybridized pores are three dimensionally interconnected as shown in Fig. 1(a).

Inherent Static Water Contact Angle (SWCA) of the ASNPS on the rod-shaped heater is $\theta \sim 72°$ as shown in Fig. 1(b). After surface treatment with the SAM coating, the SWCA of the ASNPS is modified into a hydrophobic surface, $\theta \sim 126°$.

### 2.2. Spectroscopic characterization of aqueous surfactant solution

Evolution of surfactant aggregate size was characterized by Dynamic Light Scattering (DLS) and a digital microscope. For DLS measurement, each sample with different concentrations of SDS solutions was delivered into a quartz cuvette. Hydrodynamic radius was measured at each concentration of surfactant solutions. Zetasizer Nano S (Malvern) was used in this study. Surfactant aggregate size was also confirmed with the digital microscope (Keyence VHX-100). The microscopic morphology and structure were observed by using a JEOL 2100F Transmission Electron Microscope (TEM) and a Field-Emission Scanning Electron Microscope (FE-SEM, Hitachi S-4700).

### 2.3. Pool boiling experimental setup and procedure

Nucleate pool boiling experimental setup is described elsewhere [15]. As shown in Fig. 2, dimensions of aluminum alloy (Al 6061) rod-shaped heater are 19.1 mm in diameter and 101.6 mm in length, respectively. A cartridge heater (McMaster Carr 120 V 400 W) was inserted into the rod (diameter of 9.5 mm and a length of 76.2 mm). A high thermal conductive paste (Omega 201) was used to securely contact a cartridge heater to the center hole. In order to measure wall superheat, T-type thermocouples (Omega) were used. Nominal uncertainty of T-type thermocouple was ±0.5 °C. In Fig. 2, four holes, each 2.4 mm in diameter and 70.0 mm in depth and 1.2 mm away from the heating surface, were drilled at the top, middle, and the bottom 90° apart along the periphery of the test section. T-type thermocouples (Omega) were inserted into the small peripheral holes with the high thermal conductive paste to measure the temperatures. Input power was supplied by AC variable transformer to the cartridge heater. Output voltage and current were monitored with digital multimeters (Agilent 34410A and Fluke 87V). The voltage and current measurement uncertainties were ±0.5 V and ±0.04 A, respectively. In order to condense the vapor during pool boiling, a reflux condenser with a constant temperature controller (Polyscience) was used. Measured temperature was acquired by a data acquisition system (IOtech).

The procedure to obtain experimental results is described in detail elsewhere [15]. The experiments were performed at the steady state under the atmospheric pressure condition. The pool temperature is maintained within 0.8 °C of $T_{sat}$. The estimated uncertainties of power input and heat flux were within 8.4 and 9.7%, respectively.

## 3. Results and discussion

### 3.1. Surfactant-induced surface wetting change on porous surfaces

In general, surfactants consist of a water-soluble (hydrophilic) part and a water-insoluble (hydrophobic) part. The hydrophobic part is a saturated hydrocarbon chain, whereas the hydrophilic part is generally ionizable and belongs to a polar group, which can form hydrogen bonding network in an aqueous solution [17]. As schematically illustrated in Fig. 3(a), the hydrophobic part of

**Table 1**
Pool boiling heat transfer enhancement in various surfactant solutions.

| References | Boiling regimes | Heating surface/shape | Fluid | HTC improvement |
|---|---|---|---|---|
| Tzan [4] | Nucleate | Nickel plated copper Tube | SDS in water | 133% |
| Wu [5] | CHF | Copper sphere | SDS/SLBS in water | 30% |
| Ammerman [6] | Nucleate | Copper wire | SDS in water | 45% |
| Wu [7] | Nucleate | Stainless steel tube | SDS/Triton X-100 in water | 100% |
| Wen [8] | Nucleate | Copper plate | SDS/Triton X-100 in water | 80–190% |
| Wasekar [9] | Nucleate | Gold plated copper tube | SDS/SLES/Triton X-100 in water | 50–70% |
| Kathiravan [10] | CHF | Copper sputtered tube | Copper nanofluid | 59% |
| Peng [11] | Nucleate | Copper plate | R113 | 60–100% |

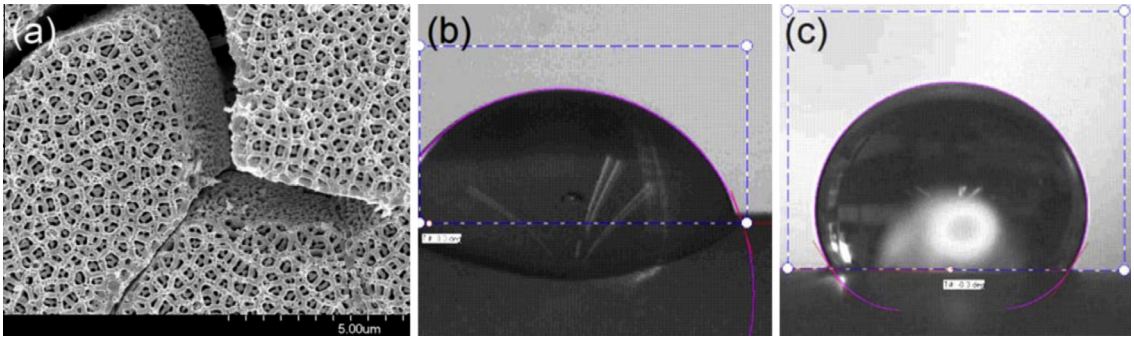


**Fig. 1.** (a) FE-SEM image of the ASNPS, (b) SWCA of the ASNPS (hydrophilic) on the rod-shaped heater ($\theta \sim 72°$) and (c) WCA of the SASNPS (hydrophobic) on the rod-shaped heater ($\theta \sim 126°$).

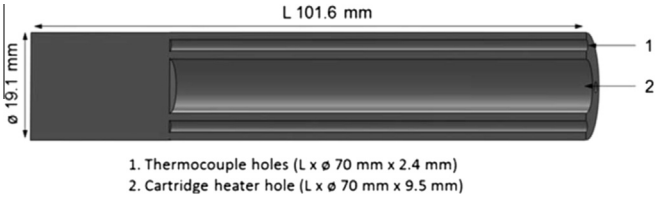


**Fig. 2.** Cross-sectional view of Al 6061 heater section used for pool boiling experiments.

surfactant is represented as a long (red) chain, while the hydrophilic part is described as a solid (red) circle. Depending on the hydrophilic part, surfactants are categorized into cationics (fatty nitriles and amines), anionics (carboxylic acids, sulfuric esters, and sulfonates), and non-ionics (polyethoxy and polyhydroxy groups). Since those parameters are closely related to the diffusion of each molecule, diffusion is much faster towards the vapor–liquid interface at higher concentrations and temperature. The molecular motion (rotation and translation) in liquid is influenced by the size of surfactants. For a surfactant with larger molecular weight, it takes much longer equilibrium time in surface tension relaxation than smaller ones. Also, it is important to note that the surface tension of the liquid is inversely proportional to the additive concentration of surfactants and the temperature of the solution.

In this study, the well-known anionic and nonionic surfactants, (SDS (Sodium Dodecyl Sulfate) and Triton X-100) were used in the pool boiling experiment. As illustrated in Fig. 3(b), SDS consists of a hydrophobic tail and a hydrophilic head. The hydrophobic tail $(-CH_2-)_n$ is chemically inert. The hydrophilic head is a polarizable sulfonate ($-SO_2O-$) group, which easily forms hydrogen bonding in an aqueous solution. Similarly, Triton X-100 has a hydrophobic saturated carbon and benzene and a hydrophilic ethylene oxide group $(-CH_2OCH_2-)_n$. Physicochemical properties of SDS and Triton X-100 are summarized and compared to pure water in Table 2.

The surfactant-induced hydrophilization on the hydrophilic surface is a well-known mechanism [17]. Typically, at lower concentration, individual surfactant molecules diffuse homogeneously in liquid as illustrated in Fig. 4(a). As surfactant concentration increases, the reactive polar head of the surfactant begins to adsorb on the heating surface (hemi micelle). Parallel aligned hydrophobic tails are directed toward water and they are thermodynamically destabilized due to contact with water. To avoid a thermodynamically unfavorable state, surfactant molecules aggregate in opposite direction to remove hydrophobic groups from contact with water, thereby reducing the free energy of the system (reverse hemi micelle). At this point, the hydrophilic polar head contacts with water and forms a hydrogen bonding network, which induces surface wetting. At higher concentration, fully reversed hemi micelles form a bilayer. These surfactant self-assemblies lead to substantial interfacial surface tension change. Beyond a certain concentration of

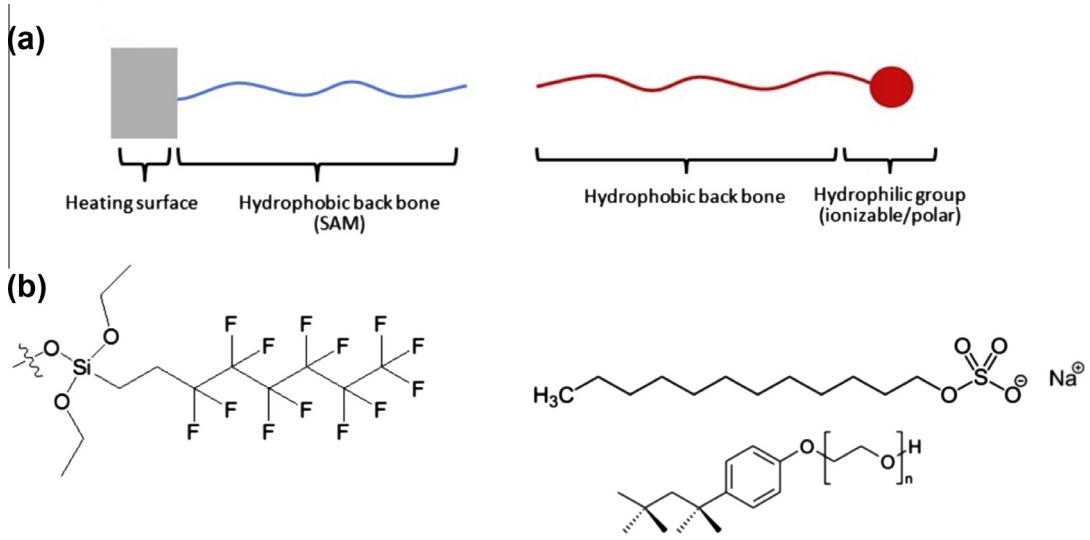


**Fig. 3.** (a) Schematic illustration of a heating surface and a surfactant and (b) molecular structures of a SAM coating (left) and surfactants (upper: SDS (Sodium Dodecyl Sulfate), $CH_3(CH_2)_{11}OSO_3Na$, Lower: Triton X-100, $t$-Oct-$C_6H_4$-$(OCH_2CH_2)_{10}OH$).

**Table 2**
Physicochemical properties of surfactants vs. water.

| Surfactant | Water | SDS | Triton X-100 |
|---|---|---|---|
| Chemical formula | $H_2O$ | $C_{12}H_{15}SO_4$ | $C_{14}H_{21}(OCH_2CH_2)_{9-10}OH$ |
| Ionic nature | Neutral | Anionic | Nonionic |
| Molecular weight | 18 | 288 | 624 (average) |
| CMC | – | 2500 wppm | 200 wppm |
| Surface tension | 72.75 mN/m | 36 mN/m (1 wt.%) | 30 mN/m (1 wt.%) |
| Viscosity | 0.32 cps | – | 240 cps |

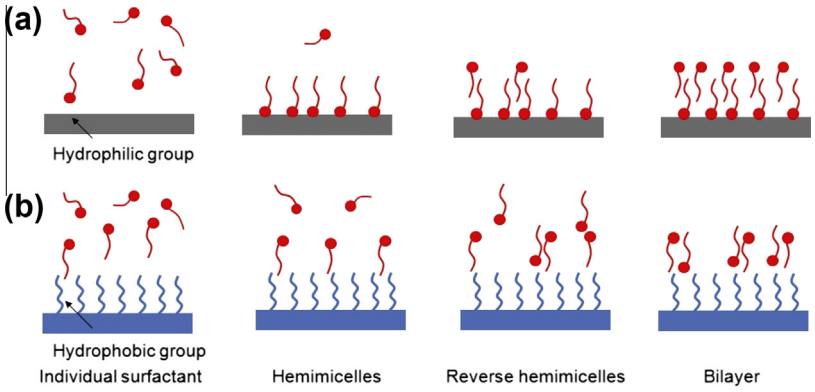


**Fig. 4.** Schematic illustration of surfactants physisorption process on heating surfaces with different wetting: (a) hydrophilic and (b) hydrophobic heating surfaces. At lower concentrations, surfactants are dispersed in liquid. As concentration increases, surfactants form hemimicelles, reverse hemimicelle, and bilayer on the heating surface.

surfactants, the asymptotic limit of surface tension is reached. It is called Critical Micelle Concentration (CMC), which is characterized by aggregates of surfactant molecules [17].

In this study, surfactant physisorption process would be different from the hydrophilic surface case since the heating surface (ASNPS: hydrophilic) wetting was modified with a hydrophobic SAM coating (SASNPS: hydrophobic). Similarly, at lower concentrations, individual molecules diffuse in liquid in Fig. 4(b). Adsorption reactivity of polar groups on the hydrophobic surface would not be significant due to the low surface energy coating. Once some of them are adsorbed onto the heating surface, the hydrophobic surface becomes wet since the bilayer interacts with water. Therefore, it is assumed that much longer time is required to change the surface wetting on the hydrophobic surface.

In Fig. 5, Static Water Contact Angle (SWCA) of SDS and Triton X-100 was measured on the different wetting surfaces (ASNPS and SASNPS). For SASNPS-SDS, the SWCA rarely decreases ($\theta_{SDS}/\theta_{water} < 5\%$) at lower concentrations (<500 wppm). As concentration increases near CMC (2500 wppm), the SWCA reaches a plateau to the hydrophobic regime ($\theta \sim 110°$). The SWCA trend implies that surfactant aggregates are not easily adsorbed on the hydrophobic SAM coating and cannot yield instant wetting. For ASNPS-SDS, appreciable SWCA decrease ($\theta_{SDS}/\theta_{water} > 50\%$) is observed as surfactant concentration increases. This phenomenon can be explained by surfactant affinity over the hydrophilic ASNPS and it leads to instant wetting change.

From the SWCA measurements in Fig. 5, general ideas of surfactant-induced wetting phenomena on the hydrophobic surface are provided. In order to understand immediate interfacial tension at the bubble rim, dynamic interplays between inertia of the droplet, surface tension, and viscous dissipation need to be elucidated. Gätne [18] suggested a drop impact test to capture the underlying physics of instant wetting phenomena. The time scale to reach equilibrium at the newly formed three phase interface during boiling is of the same order (~100 ms) as that for the drop impact test [18]. Therefore, information of instantaneous wetting obtained during the drop impact test in Fig. 6(b) may give a clue to understand interfacial wetting behavior during bubble ebullience as illustrated in Fig. 6(a).

In Fig. 7, the high speed camera images during the drop impact test on the hydrophobic surface (SASNPS) were visualized. Once a drop impacts and spreads on the solid surface, surface tension of liquid decelerates its spreading. The droplet rim reaches its maximum diameter when the contact line speed reaches zero. This is called the "relaxation phase". The initial kinetic energy of the drop converts into viscous dissipation. If the surface tension of the liquid is sufficient, the contact line immediately retracts to a smaller final diameter.

For pure water, the maximum spread is shown in 3 ms, which is less than the time required to adsorb onto the porous surface in Fig. 7(a). Therefore, the SASNPS would repel the water droplet, which would swiftly retract due to strong surface tension. However, a significant WCA hysteresis at the droplet contact rim prohibits immediate columnar recoil/rebound [19]. The WCA hysteresis was visualized by dipping and withdrawing the SASNPS slab in water (Fig. S1). Interplay of undissipated kinetic energy and a droplet pinning yields the formation of a small droplet, which is separated from a base droplet (6 ms). It is assumed that its kinetic energy is not thoroughly consumed through viscous dissipation.

A droplet of a SDS 500 wppm solution shows spreading and recoil but a droplet separation is not observed in Fig. 7(b). This might be caused by viscosity increase. Once a flat disc-shaped droplet impinges, as shown for 2 ms, a droplet interface instantly retracts and an abacus-shaped droplet is observed (3 ms). Compared to the image (4 ms) in Fig. 7(a), a droplet contact area of SDS 500 wppm is much smaller. Its interface swiftly retracts up to 5 ms and it repeats spreading and recoil. It implies that liquid hardly impregnates into the porous surface and instantaneous wetting rarely occurs within a limited time (<10 ms).

As surfactant concentration increases (SDS 2500 wppm), a droplet shows a maximum diameter spreading and minimum height at relaxation phase (2 ms) in Fig. 7(c). It rarely shows recoil and rebound due to instant wetting, which is induced by reduced surface tension and enhanced viscosity.

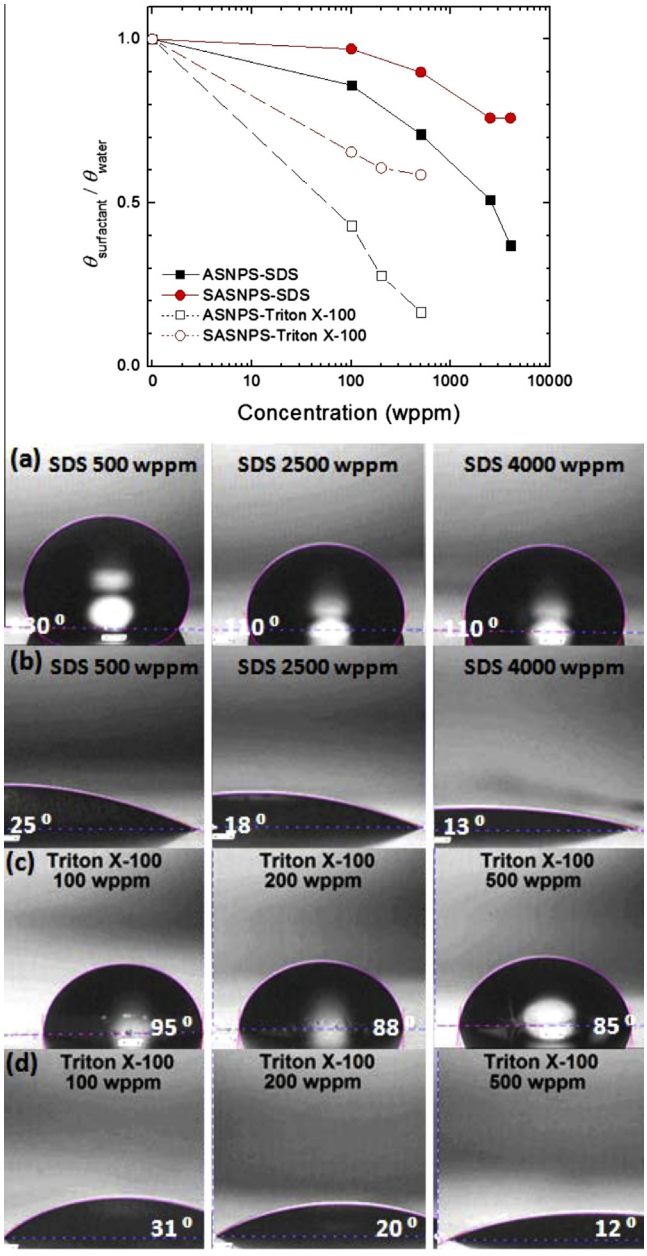


**Fig. 5.** Static water contact angle (SWCA) measurements of various surfactants on the porous structures: (a) SASNPS-SDS, (b) ASNPS-SDS, (c) SASNPS-Triton X-100 and (d) ASNPS-Triton X-100.

Surfactant aggregation behaviors in an aqueous SDS solution were investigated by spectroscopic methods such Dynamic Light Scattering (DLS) and Transmission Electron Microscopy (TEM) in Fig. 8. In general, DLS is used to analyze hydrodynamic radius of nano particles and aggregates at nanometer level. The distribution of Hydrodynamic Radius (HR) at various SDS concentrations is shown in Fig. 8(a). The HR at SDS 100 wppm is approximately 2–3 nm. It implies that individual molecules do exist in the form of unimers. At SDS 500 wppm, mean HR of aggregates is around 150 nm. As concentration increases, aggregates HR increases and eventually, form micelles. Above 1000 wppm, micelle HR is a few micrometers (3–10 μm), which is much larger than the radius of nano pores. Probably, bubble growth at the nano pores might be influenced by the micelle formation.

Concomitantly, microscope analysis and TEM study were conducted. In Fig. 8(b), a digital microscope image of SDS 2500 wppm reveals surfactant micellar aggregates with a diameter of 3–7 μm, which is consistent with DLS analysis in Fig. 8(a). Similarly, a TEM image in Fig. 8(c) confirms that the surfactant forms micellar aggregates near CMC.

### *3.2. Nucleate pool boiling of the SASNPS (hydrophobic) in aqueous surfactant solutions*

In Section 3.1, surfactant-induced liquid property change is characterized by various physical and optical methods. Effectiveness of additive surfactants in the pool boiling phenomena is clearly shown in Fig. 9(a). Compared to the reference (a plain surface in water), the SASNPS shows a huge wall superheat decrease ($\Delta\Delta T \sim 5$ K, −104%). As the concentration of aqueous SDS solutions increases up to 500 wppm, Onset of Nucleate Boiling (ONB) is substantially reduced (<1 K). Overall wall superheat reduction is huge at the given heat flux ($\Delta\Delta T \sim 8$ K). This phenomenon is represented by the characteristic leftward shift of a boiling curve relative to the reference curve. Above SDS 500 wppm, heat transfer deteriorates. Beyond CMC, there is no further heat transfer deterioration observed in Fig. 9(a).

One thing to note in Fig. 9(a) is that the boiling curves do not show heat transfer deterioration even at higher heat flux regimes. In pure water, the significant heat transfer augment at lower heat flux regimes (<40 kW/m$^2$) is assumed by the active nucleation site increase and the Liquid Thin Film Evaporation (LTFE) [15,20]. At high heat flux regimes (>60 kW/m$^2$), bubble coalescence influences the heat transfer deterioration due to a bubble blanketing.

The enhanced boiling heat transfer phenomena are reflected in Heat Transfer Coefficient (HTC) in Fig. 9(b). For pure water, the SASNPS shows overall 104% HTC enhancement (overall HTC 19.9 kW/m$^2$K) compared to the reference (plain surface in water).

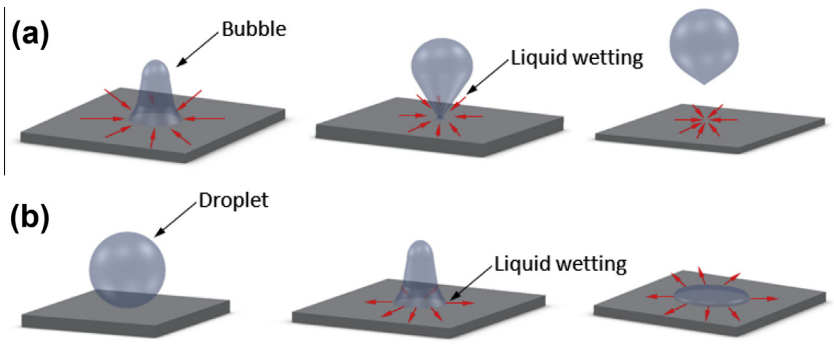


**Fig. 6.** Schematic illustration of instantaneous wetting change at three-phase interface: (a) liquid impingement during bubble nucleations and (b) liquid impingement during drop impact. A red arrow represents three phase interfacial tension. (For interpretation of the references to color in this figure legend, the reader is referred to the web version of this article.)

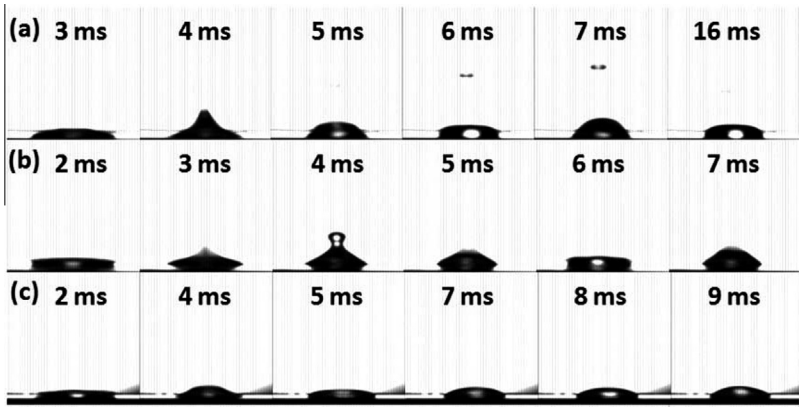


**Fig. 7.** Drop shape evolution ($Re = 30$) on the SASNPS during drop impact for various liquids: (a) Water, (b) SDS 500 wppm and (c) SDS 2500 wppm.

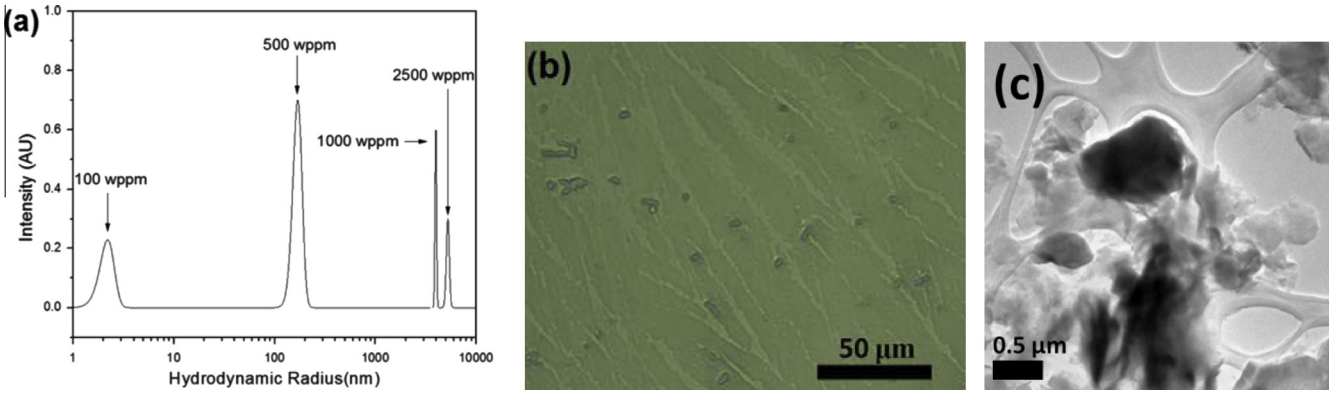


**Fig. 8.** (a) Hydrodynamic radius of aqueous SDS solutions with different concentrations (100–2500 wppm), (b) a digital microscopic image and (c) TEM image of SDS aggregates in SDS 2500 wppm solution.

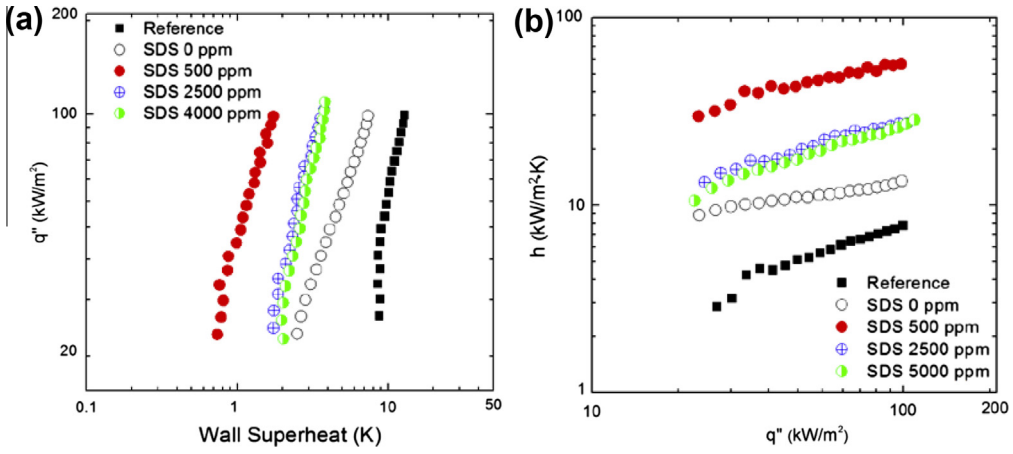


**Fig. 9.** Boiling curves of the SASNPS in aqueous SDS solutions with different concentrations (0–4000 wppm) (a) $q''$ vs. $\Delta T$ and (b) $q''$ vs. $h$.

At SDS 500 wppm, the overall HTC (45.1 kW/m$^2$ K) is dramatically improved and approximately 7.3 times enhancement is achieved compared to the reference. This value is significantly large and has never been reported yet in pool boiling heat transfer. As surfactant concentration increases above SDS 500 wppm, heat transfer steadily deteriorates. At SDS 2500 wppm (CMC), the overall HTC (21.3 kW/m$^2$ K) decreases almost by half compared to HTC at SDS 500 wppm. However, this value is still 2.8 times higher than that in pure water in Fig. 9(b).

In order to understand heat transfer enhancement relating to bubble motion, pool boiling visualization is shown in Fig. 10. Compared to the reference in Fig. 10(a), the SASNPS in water shows significant bubble ebullience over the entire heating surface due to numerous active nucleation sites in Fig. 10(b). Wang and Dhir have proven that a hydrophobic heating surface increases the number of active nucleation sites [21]. Since a hydrophobic SAM coating yields interfacial tension change and reduces $\sigma_{SL}$ in Young–Laplace equation ($cos\ \theta = (\sigma_{SV} - \sigma_{SL})/\sigma_{LV}$), bubble coalescence is

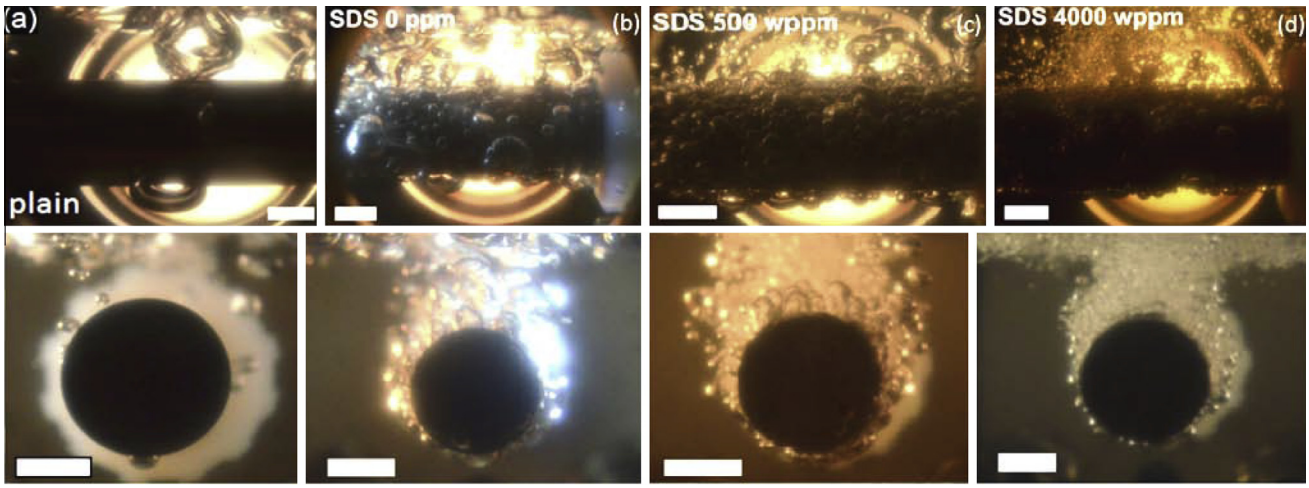


**Fig. 10.** Visualization of bubble ebullience on the SASNPS in various liquids (SDS 0–4000 wppm) at $q''$ = 20 kW/m$^2$: (a) plain surface in SDS 0 wppm, (b) the SASNPS in SDS 0 wppm, (c) the SASNPS in SDS 500 wppm and (d) the SASNPS in SDS 4000 wppm. Scale bar represents 9 mm.

pronounced leading to wall superheat increase on the SASNPS. In general, after a large bubble lift-off, liquid is pumped in and out through interconnected passages, which facilitate fresh liquid into the porous media by liquid intake process. The fresh liquid infiltration reduces the wall superheat even at high heat flux region. However, for pure water, it takes longer relaxation time in instantaneous liquid impregnation on the SASNPS as shown in Fig. 7(a). Fresh liquid infiltration might be retarded and/or prevented by poor wetting at the pore mouth (SASNPS).

In SDS 500 wppm solution, bubble diameter becomes smaller in Fig. 10(c) since additive surfactant leads to interfacial tension change, which prevents bubble coalescence. One thing to note in substantially enhanced heat transfer performance is a combination of large and small size bubbles, which is simultaneously observed as shown in Fig. S2. A larger bubble leads to enhanced internal and external convection-driven heat transfer. A smaller bubble concomitantly increases bubble departure frequency. Eventually, significant bubble ebullience achieves dramatic HTC enhancement in Fig. 9.

At or above CMC (2500–4500 wppm), bubble diameter becomes appreciably small and tiny bubbles along the heater periphery are observed in Fig. 10(d). Although the bubble departure frequency at high concentrations of SDS surfactant increases, the latent heat removal due to internal and external convection induced by tiny bubbles may be much smaller than that in SDS 500 wppm. Also, excess amount of the surfactant reduces interfacial tension at the bubble rim and leads to instant wetting in Fig. 7(c). It implies that after bubble lift-off, the liquid advances instantly into active cavities. Nucleation sites become wet and inactive. Therefore, boiling incipience commences at higher wall superheat and heat transfer deterioration at higher concentration is observed in Fig. 9(a).

Nakayama and Webb introduced the "suction-evaporation" mechanism [22–24] to explain heat transfer at the active cavities. In pure water, when pumping motions are generated, liquid may not advance along the cavity mouth due to enhanced interfacial tension on the hydrophobic surface (see Fig. S1(a)). Pumping motions-induced fresh liquid infiltration may be prohibited. Therefore, internal convection portion may not be significant. Also, WCA hysteresis prevents liquid hovering on the SASNPS in Fig. 7(a). A combined effect might increase wall superheat.

As surfactant concentration increases, surfactant molecules diffuse preferably at the adjacent bubble rim and yields smaller bubbles. At SDS 500wppm, it seems that the WCA hysteresis at the droplet base rim decreases in Fig. S1(b). The reduced WCA hysteresis enables liquid to advance and recede on the SASNPS during an oscillating motion of the droplet shape between an abacus (the droplet base is rarely wet) and a disc as shown in Fig. 7(b). It implies that the liquid might move back and forth during liquid pumping in and out through porous media. Instantaneously dry and wet cavities can take advantage in heat transfer: First, liquid in and out removes its latent heat from the heating surface during pumping motions. Second, dry cavities still remain active and bubble residue (dotted line on the cavity) reduces bubble waiting time, which is illustrated in Fig. 11(a). Third, at some menisci, the LTFE might occur and contribute to heat transfer augment.

At higher concentrations, surfactant aggregates would show fast diffusion along the bubble rim. Enhanced wetting due to surfactants would lead the liquid to permeate into the substructure when negative pressure develops. As schematically illustrated in Fig. 11(b), an adjacent cavity becomes wet and deactivated. Drop impact test in Fig. 7(c) confirms that surfactant aggregates induce instantaneous wetting.

Up to now, the pool boiling enhancement in ionic surfactant (SDS) solutions has been discussed. Under the same condition,

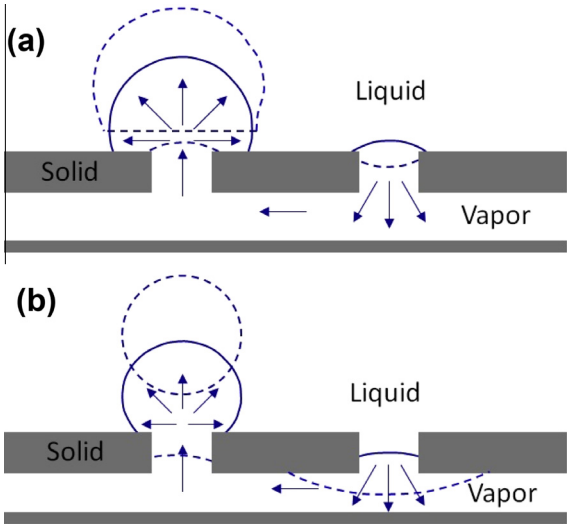


**Fig. 11.** The Suction-evaporation modes on the hydrophobic porous surface in aqueous surfactant solutions: (a) SDS < 500 wppm and (b) SDS > 2500 wppm. Dotted line represents the liquid boundary after bubble lift-off. Arrows symbolize the vapor pressure.

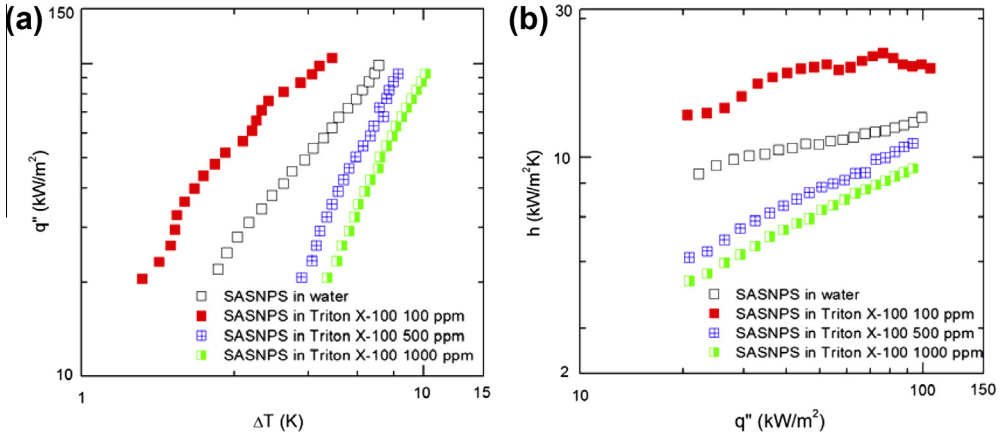


**Fig. 12.** Boiling curves of the SASNPS in aqueous Triton X-100 solutions (0–1000 wppm) (a) $q''$ vs. $\Delta T$ (b) $q''$ vs. $h$.

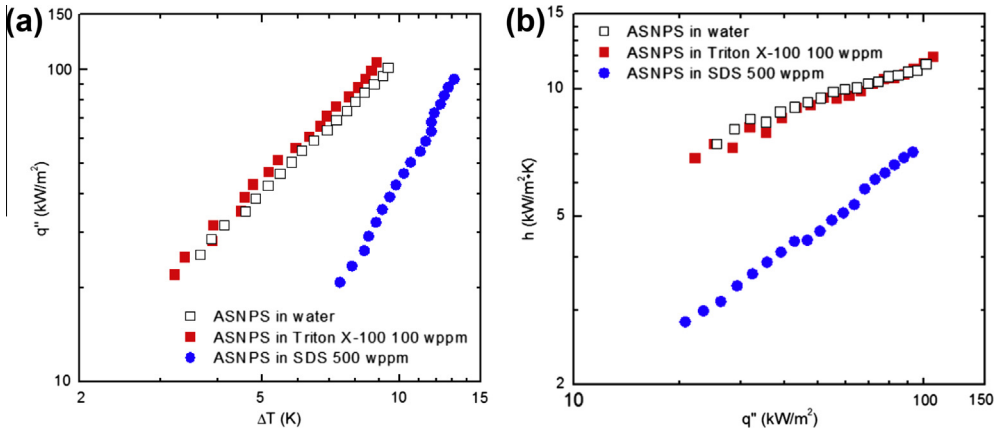


**Fig. 13.** Boiling curves of the ASNPS in aqueous SDS (500 wppm) and Triton X-100 (100 wppm) solutions (a) $q''$ vs. $\Delta T$ (b) $q''$ vs. $h$.

the boiling performance in non-ionic surfactant (Triton X-100) was tested. By addition of the small amount of Triton X-100 (100 wppm), the boiling curve shows heat transfer augment in Fig. 12(a). Overall HTC enhancement in Fig. 12(b) is less than SDS cases. As surfactant concentration increases, the boiling curves suddenly move to the right and significant heat transfer deterioration is observed. In higher concentration solution (>200 wppm), obvious heat transfer deterioration at the lower heat flux regime is observed (<60 kW/m$^2$). From these phenomena it is assumed that surfactant aggregates near and/or above the CMC (200 wppm) influence wetting on the SASNPS. Surfactant-induced wetting (SASNPS-Triton X-100) shows more dramatic trends than shown in the SWCA in Fig. 5. Since Triton X-100 has a more polarizable ethylene oxide group $(-CH_2OCH_2-)_n$ than the saturated carbon backbone $(-CH_2-)_n$ in SDS, even at 100 wppm, the ratio of $\theta_{surfactant}/\theta_{water}$ is close to 50% due to substantial instantaneous wetting. The enhanced wetting assists liquid to permeate into the active cavities and reduces the number of the active sites. For the fully wetted cavities, more heat is required to commence incipient boiling [25] and heat dissipation through the LTFE does not occur.

### 3.3. Nucleate pool boiling of the ASNPS (hydrophilic) in aqueous surfactant solutions

In Section 3.2, pool boiling heat transfer of the SASNPS (a hydrophobic surface) in aqueous surfactant solutions is shown. In order to observe the influence of the heating surface wettability in aqueous surfactant solutions, pool boiling tests were carried out at the optimum concentration of individual surfactant solutions on the ASNPS (hydrophilic): SDS 500 wppm and Triton X-100 100 wppm. For the SDS 500 wppm solution, the pool boiling curve moves far right and the HTC decreases by 50% compared to that in pure water in Fig. 13(a). Relating surface wetting to the SWCA in Fig. 5(b), it is assumed that SDS surfactant molecules diffuse faster and its polar head $(-SO_2O-)$ is easily adsorbed onto the heating surface through hydrogen bonding. Therefore, liquid swiftly impregnates into porous wicks and floods the nucleation site. Surface wetting-induced homogeneous boiling requires more heat to initiate the bubble nucleation [25].

On the contrary, pool boiling curve in Triton X-100 100 wppm solution does not show substantial change in Fig. 13(a). It implies that individual Triton X-100 molecules diffuse in aqueous solution and they are not adsorbed on the ASNPS. Compared to SDS, Triton X-100 has significant difference: First, the Triton X-100 does not have an active polar (ionic) head in Fig. 3(b). Therefore, it cannot make a hydrogen bonding network, which enhances the surface wetting. Second, the size of Triton X-100 is longer and much bulkier than that of the SDS molecule. Molecular motions of Triton X-100 in aqueous solution are limited and diffusion might be retarded. It means that Triton X-100 requires much longer time to reach equilibrium between liquid and the heating surface at the given conditions.

## 4. Conclusions

In this study, the interfacial wetting phenomena were compared in (non)ionic polymeric liquids. The following conclusions are summarized:

1. For the SASNPS (hydrophobic), ionic surfactant (SDS) boosted heat transfer by reducing bubbles departure frequency, coalescence, and the suction-evaporation mode. At the optimal concentration, a combined effect achieved dramatic heat transfer enhancement. Beyond the optimal concentration, heat transfer deteriorated due to instantaneous liquid impingement and tiny bubbles, which decreased internal and external convective flows.
2. On the contrary, heat transfer augmentation in non-ionic surfactant (Triton X-100) solution was not significant due to instantaneous wetting of the active cavities. It was assumed that the flexible ethoxy group in Triton X-100 would diffuse and assist intermolecular interactions.
3. For the ASNPS (hydrophilic), immediate wetting phenomena were much significant due to enhanced diffusion and wetting through hydrogen bonding It yielded instantaneous liquid impregnation into the active cavities and deteriorated heat transfer performance.

## Acknowledgement

This material is based upon work supported by the National Science Foundation under Grant No. 0923869 (STTR Phase II through Advanced Materials and Devices Inc., Reno, NV). Also, KJK thanks Southwest Gas Corporation for their generous support for his research.

## Appendix A. Supplementary data

Supplementary data associated with this article can be found, in the online version, at http://dx.doi.org/10.1016/j.ijheatmasstransfer.2013.03.064.

## References

[1] W. Frost, C.J. Kippenhan, Bubble growth and heat transfer mechanisms in the forced convection boiling of water containing a surface active reagent, Int. J. Heat Mass Transfer 10 (1967) 931–949.
[2] P. Kotchaphakdee, M.C. Williams, Enhancement of nucleate pool boiling with polymeric additives, Int. J. Heat Mass Transfer 13 (1970) 835–848.
[3] G. Heteroni, M. Gurevich, A. Mosyak, R. Rozenblit, Z. Segal, Boiling enhancement with environmentally acceptable surfactants, Int. J. Heat Fluid Flow 25 (2004) 841–848.
[4] Y.L. Tzan, Y.M. Yang, Experimental study of surfactant effects on pool boiling heat transfer, ASME J. Heat Transfer 112 (1990) 207–212.
[5] W.T. Wu, H.S. Lin, Y.M. Yang, Critical heat flux in pool boiling of aqueous surfactant solutions as determined by the quenching method, Int. J. Heat Mass Transfer 37 (1994) 2377–2379.
[6] C.N. Ammerman, S.M. You, Determination of the boiling enhancement mechanism caused by surfactant addition to water, ASME J. Heat Transfer 118 (1996) 429–435.
[7] W.T. Wu, Y.M. Yang, J.R. Maa, Nucleate pool boiling enhancement by means of surfactant additives, Exp. Therm. Fluid Sci. 18 (1998) 195–209.
[8] D.S. Wen, B.X. Wang, Effects of surface wettability on nucleate pool boiling heat transfer for surfactant solutions, Int. J. Heat Mass Transfer 45 (2002) 1739–1747.
[9] V.M. Wasekar, R.M. Manglik, The influence of additive molecular weight and ionic nature on the performance of aqueous surfactant solutions, Int. J. Heat Mass Transfer 45 (2002) 483–493.
[10] R. Kathiravan, R. Kumar, A. Guptak, R. Chandra, Characterization and pool boiling heat transfer studies of nanofluids, ASME J. Heat Transfer 1331 (2009) 081902.
[11] H. Peng, G. Ding, H. Hu, Effect of surfactant additives on nucleate pool boiling heat transfer of refrigerant-based nanofluid, Exp. Therm. Fluid Sci. 35 (2011) 960–970.
[12] R.M. Manglik, V.M. Wasekar, J. Zhang, Dynamic and equilibrium surface tension of aqueous surfactant and polymeric solutions, Exp. Therm. Fluid Sci. 25 (2001) 55–64.
[13] J. Zhang, R.M. Manglik, Effect of ethoxylation and molecular weight of cationic surfactants on nucleate boiling in aqueous solutions, ASME J. Heat Transfer 126 (2004) 34–42.
[14] J. Zhang, R.M. Manglik, Additive adsorption and interfacial characteristics of nucleate pool boiling in aqueous surfactant solutions, ASME J. Heat Transfer 127 (2005) 684–691.
[15] B.J. Zhang, K.J. Kim, H.K. Yoon, Enhanced heat transfer performance of alumina sponge-like nano-porous structures through surface wettability control in nucleate pool boiling, Int. J. Heat Mass Transfer (in press).
[16] B.J. Zhang, K.J. Kim, Effect of liquid uptake on critical heat flux utilizing a three dimensional, interconnected alumina nano porous surface, Appl. Phys. Lett. 101 (2012) 054104.
[17] B. Holmberg, B. Jönsson, B. Kronberg, Lindman, Surfactants and Polymers in Aqueous Solution, second ed., John Wiley & Sons, LTD., West Sussex, England, 2003. pp. 389–420.
[18] K.P. Gätne, M.A. Jog, R.M. Manglik, Surfactant-induced modification of low weber number droplet impact dynamics, Langmuir 25 (2009) 8122–8130.
[19] D. Richard, C. Clanet, D. Quére, Contact time of a bouncing drop, Nature 417 (2002) 811.
[20] M.A. Hanlon, H.B. Ma, ASME J. Heat Transfer 125 (2003) 644.
[21] C.H. Wang, V.K. Dhir, Effect of surface wettability on active nucleation site density during pool boiling of water on a vertical surface, ASME J. Heat Transfer 115 (1993) 659–669.
[22] W. Nakayama, T. Daikoku, H. Kuwahara, T. Nakajima, Dynamic model of enhanced boiling heat transfer on porous surfaces, ASME J. Heat Transfer 102 (1980) 445–450.
[23] W. Nakayama, T. Daikoku, T. Nakajima, Effect of pore diameters and system pressure on saturated pool nucleate boiling heat transfer from porous surfaces, ASME J. Heat Transfer 104 (1982) 286–291.
[24] R.L. Webb, Principles of Enhanced Heat Transfer, John Wiley & Sons, New York, 1994.
[25] V.P. Carey, Liquid–Vapor Phase Change Phenomena, Hemisphere publishing corp., Washington, 1992. pp. 176–186.